Northumbria Research Link

This version was downloaded from Northumbria Research Link: http://nrl.northumbria.ac.uk/13380/

www.northumbria.ac.uk/nrl

northumbria
UNIVERSITY
University Library

A new sinusoidal shear deformation theory for bending, buckling, and vibration of functionally graded plates

Huu-Tai Thai [a,*], Thuc P. Vo [b,c]

[a] Department of Civil and Environmental Engineering, Hanyang University, 17 Haengdang-dong, Seongdong-gu, Seoul 133-791, Republic of Korea

[b] School of Mechanical, Aeronautical and Electrical Engineering, Glyndwr University, Mold Road, Wrexham LL11 2AW, UK.

[c] Advanced Composite Training and Development Centre, Glyndwr University, Unit 5, Hawarden Industrial Park, Deeside, Flintshire CH5 3US, UK.

Abstract

A new sinusoidal shear deformation theory is developed for bending, buckling, and vibration of functionally graded plates. The theory accounts for sinusoidal distribution of transverse shear stress, and satisfies the free transverse shear stress conditions on the top and bottom surfaces of the plate without using shear correction factor. Unlike the conventional sinusoidal shear deformation theory, the proposed sinusoidal shear deformation theory contains only four unknowns and has strong similarities with classical plate theory in many aspects such as equations of motion, boundary conditions, and stress resultant expressions. The material properties of plate are assumed to vary according to power law distribution of the volume fraction of the constituents. Equations of motion are derived from the Hamilton's principle. The closed-form solutions of simply supported plates are obtained and the results are compared with those of first-order shear deformation theory and higher-order shear deformation theory. It can be concluded that the proposed theory is accurate and efficient in predicting the bending, buckling, and vibration responses of functionally graded plates.

---

* Corresponding author. Tel.: + 82 2 2220 4154.
E-mail address: thaihuutai@hanyang.ac.kr (H.T. Thai), t.vo@glyndwr.ac.uk (T.P. Vo).

1. Introduction

Functionally graded materials (FGMs) are a class of composites that have continuous variation of material properties from one surface to another and thus eliminate the stress concentration found in laminated composites. FGMs are widely used in many structural applications such as mechanics, civil engineering, aerospace, nuclear, and automotive. In company with the increase in the application of FGM in engineering structures, many computational models have been developed for predicting the response of functionally graded (FG) plates. These models can either be developed using displacement-based theories (when the principle of virtual work is used) or displacement-stress-based theories (when Reissner's mixed variational theorem is used). In general, these theories can be classified into three main categories: classical plate theory (CPT); first-order shear deformation theory (FSDT); and higher-order shear deformation theory (HSDT).

The CPT, which neglects the transverse shear deformation effects, provides accurate results for thin plates [1-4]. For moderately thick plates, it underestimates deflections and overestimates buckling loads and natural frequencies. The FSDT accounts for the transverse shear deformation effect, but requires a shear correction factor to satisfy the free transverse shear stress conditions on the top and bottom surfaces of the plate [5-11]. Although the FSDT provides a sufficiently accurate description of response for thin to moderately thick plates, it is not convenient to use due to difficulty in determination of correct value of the shear correction factor. To avoid the use of shear correction factor, many HSDTs were developed based on the assumption of quadratic, cubic or higher-order variations of in-plane displacements through the plate thickness, notable among them are Reddy [12], Karama et al. [13], Zenkour [14-16], Xiao et al. [17], Matsunaga [18], Pradyumna and Bandyopadhyay [19], Fares et al. [20], Talha and Singh [21-22],

2

Benyoucef et al. [23], Atmane et al. [24], Meiche et al. [25], Mantari et al. [26], and Xiang et al. [27]. Among the aforementioned HSDTs, the well-known HSDTs with five unknowns include: the Reddy's theory [12], the sinusoidal shear deformation theory [14-16], the hyperbolic shear deformation theory [23-24], the exponential shear deformation theory [13, 26]. Although the HSDTs with five unknowns are sufficiently accurate to predict response of thin to thick plate, their equations of motion are much more complicated than those of FSDT and CPT. Therefore, there is a scope to develop a HSDT which is simple to use.

This paper aims to develop a simple sinusoidal shear deformation theory for bending, buckling, and vibration analyses of FG plates. This theory is based on assumption that the in-plane and transverse displacements consist of bending and shear parts. Unlike the conventional sinusoidal shear deformation theory [14-16], the proposed sinusoidal shear deformation theory contains four unknowns and has strong similarities with CPT in many aspects such as equations of motion, boundary conditions, and stress resultant expressions. Material properties of FG plate are assumed to vary according to power law distribution of the volume fraction of the constituents. Equations of motion are derived from the Hamilton's principle. The closed-form solutions are obtained for simply supported plates. Numerical examples are presented to verify the accuracy of the proposed theory in predicting the bending, buckling, and vibration responses of FG plates. It should be pointed out that Merdaci et al. [28], Ameur et al. [29], and Tounsi et al. [30] recently developed a theory that is similar with the present one. However, their works are limited to only bending problems.

2. Theoretical formulations

2.1. Basic assumptions

3

The assumptions of the present theory are as follows:

i.   The displacements are small in comparison with the plate thickness and, therefore, strains involved are infinitesimal.

ii. The transverse normal stress $\dagger_z$ is negligible in comparison with in-plane stresses $\dagger_x$ and $\dagger_y$.

iii. The transverse displacement u_3 includes two components of bending w_b and shear w_s. These components are functions of coordinates x, y, and time t only.

$$u_3\left(x,y,z,t\right)=w_b\left(x,y,t\right)+w_s\left(x,y,t\right) \tag{1}$$

iv. The in-plane displacements u_1 and u_2 consist of extension, bending, and shear components.

$$u_1=u+u_b+u_s \quad \text{and} \quad u_2=v+v_b+v_s \tag{2}$$

- The bending components u_b and v_b are assumed to be similar to the displacements given by the classical plate theory. Therefore, the expressions for u_b and v_b are

$$u_b=-z\frac{\partial w_b}{\partial x} \quad \text{and} \quad v_b=-z\frac{\partial w_b}{\partial y} \tag{3a}$$

- The shear components u_s and v_s give rise, in conjunction with w_s, to the sinusoidal variations of shear strains χ_{xz}, χ_{yz} and hence to shear stresses $\dagger_{xz}$, $\dagger_{yz}$ through the thickness h of the plate in such a way that shear stresses $\dagger_{xz}$, $\dagger_{yz}$ are zero at the top and bottom surfaces of the plate. Consequently, the expression for u_s and v_s can be given as

$$u_s=-\left(z-\frac{h}{f}\sin\frac{f\,z}{h}\right)\frac{\partial w_s}{\partial x} \quad \text{and} \quad v_s=-\left(z-\frac{h}{f}\sin\frac{f\,z}{h}\right)\frac{\partial w_s}{\partial y} \tag{3b}$$

2.2. Kinematics

Based on the assumptions made in the preceding section, the displacement field can be obtained using Eqs. (1)-(3) as

$$u_1\left(x,y,z,t\right)=u\left(x,y,t\right)-z\frac{\partial w_b}{\partial x}-f\frac{\partial w_s}{\partial x}$$

$$u_2\left(x,y,z,t\right)=v\left(x,y,t\right)-z\frac{\partial w_b}{\partial y}-f\frac{\partial w_s}{\partial y} \tag{4}$$

$$u_3\left(x,y,z,t\right)=w_b\left(x,y,t\right)+w_s\left(x,y,t\right)$$

where

$$f=z-\frac{h}{f}\sin\frac{f\,z}{h} \tag{5}$$

The kinematic relations can be obtained as follows:

$$\begin{Bmatrix} \epsilon_x \\ \epsilon_y \\ \gamma_{xy} \end{Bmatrix} = \begin{Bmatrix} \epsilon_x^0 \\ \epsilon_y^0 \\ \gamma_{xy}^0 \end{Bmatrix} + z \begin{Bmatrix} \kappa_x^b \\ \kappa_y^b \\ \kappa_{xy}^b \end{Bmatrix} + f \begin{Bmatrix} \kappa_x^s \\ \kappa_y^s \\ \kappa_{xy}^s \end{Bmatrix}, \begin{Bmatrix} \gamma_{yz} \\ \gamma_{xz} \end{Bmatrix} = g \begin{Bmatrix} \gamma_{yz}^s \\ \gamma_{xz}^s \end{Bmatrix} \tag{6}$$

where

$$\begin{Bmatrix} \epsilon_x^0 \\ \epsilon_y^0 \\ \gamma_{xy}^0 \end{Bmatrix} = \begin{Bmatrix} \dfrac{\partial u}{\partial x} \\[2mm] \dfrac{\partial v}{\partial y} \\[2mm] \dfrac{\partial u}{\partial y}+\dfrac{\partial v}{\partial x} \end{Bmatrix}, \begin{Bmatrix} \kappa_x^b \\ \kappa_y^b \\ \kappa_{xy}^b \end{Bmatrix} = \begin{Bmatrix} -\dfrac{\partial^2 w_b}{\partial x^2} \\[2mm] -\dfrac{\partial^2 w_b}{\partial y^2} \\[2mm] -2\dfrac{\partial^2 w_b}{\partial x\partial y} \end{Bmatrix}, \begin{Bmatrix} \kappa_x^s \\ \kappa_y^s \\ \kappa_{xy}^s \end{Bmatrix} = \begin{Bmatrix} -\dfrac{\partial^2 w_s}{\partial x^2} \\[2mm] -\dfrac{\partial^2 w_s}{\partial y^2} \\[2mm] -2\dfrac{\partial^2 w_s}{\partial x\partial y} \end{Bmatrix}, \begin{Bmatrix} \gamma_{yz}^s \\ \gamma_{xz}^s \end{Bmatrix} = \begin{Bmatrix} \dfrac{\partial w_s}{\partial y} \\[2mm] \dfrac{\partial w_s}{\partial x} \end{Bmatrix} \tag{7}$$

$$g=1-\frac{df}{dz}=\cos\left(\frac{f\,z}{h}\right)$$

2.3. Constitutive equations

The material properties of FG plate are assumed to vary continuously through the thickness of the plate in accordance with a power law distribution as

$$P\left(z\right)=P_m+\left(P_c-P_m\right)\left(\frac{1}{2}+\frac{z}{h}\right)^p \tag{8}$$

where P represents the effective material property such as Young's modulus E and mass density ρ, subscripts m and c represent the metallic and ceramic constituents,

respectively; and p is the volume fraction exponent. The value of p equal to zero represents a fully ceramic plate, whereas infinite p indicates a fully metallic plate. Since the effects of the variation of Poisson's ratio ν on the response of FG plates are very small [31-32], the Poisson's ratio ν is usually assumed to be constant. The linear constitutive relations of a FG plate can be written as

$$
\begin{Bmatrix} \sigma_x \\ \sigma_y \\ \sigma_{xy} \\ \sigma_{yz} \\ \sigma_{xz} \end{Bmatrix} = \frac{E(z)}{1-\nu^2}
\begin{bmatrix}
1 & \nu & 0 & 0 & 0 \\
\nu & 1 & 0 & 0 & 0 \\
0 & 0 & \frac{(1-\nu)}{2} & 0 & 0 \\
0 & 0 & 0 & \frac{(1-\nu)}{2} & 0 \\
0 & 0 & 0 & 0 & \frac{(1-\nu)}{2}
\end{bmatrix}
\begin{Bmatrix} \varepsilon_x \\ \varepsilon_y \\ \gamma_{xy} \\ \gamma_{yz} \\ \gamma_{xz} \end{Bmatrix}
\tag{9}
$$

2.4. Equations of motion

Hamilton's principle is used herein to derive the equations of motion. The principle can be stated in analytical form as [33]

$$
0 = \int_0^T \left(\delta U + \delta V - \delta K \right) dt
\tag{10}
$$

where δU is the variation of strain energy; δV is the variation of potential energy; and δK is the variation of kinetic energy.

The variation of strain energy of the plate is calculated by

$$
\begin{aligned}
\delta U &= \int_V \left(\sigma_x \delta\varepsilon_x + \sigma_y \delta\varepsilon_y + \sigma_{xy}\delta\gamma_{xy} + \sigma_{yz}\delta\gamma_{yz} + \sigma_{xz}\delta\gamma_{xz} \right) dA\,dz \\
&= \int_A \left\{ N_x \frac{\partial \delta u}{\partial x} - M_x^b \frac{\partial^2 \delta w_b}{\partial x^2} - M_x^s \frac{\partial^2 \delta w_s}{\partial x^2} + N_y \frac{\partial \delta v}{\partial y} - M_y^b \frac{\partial^2 \delta w_b}{\partial y^2} - M_y^s \frac{\partial^2 \delta w_s}{\partial y^2} \right. \\
&\quad \left. + N_{xy}\left(\frac{\partial \delta u}{\partial y} + \frac{\partial \delta v}{\partial x} \right) - 2M_{xy}^b \frac{\partial^2 \delta w_b}{\partial x \partial y} - 2M_{xy}^s \frac{\partial^2 \delta w_s}{\partial x \partial y} + Q_{yz}\frac{\partial \delta w_s}{\partial y} + Q_{xz}\frac{\partial \delta w_s}{\partial x} \right\} dA
\end{aligned}
\tag{11}
$$

where N, M, and Q are the stress resultants defined as

$$
\left(N_i, M_i^b, M_i^s \right) = \int_{-h/2}^{h/2} (1, z, f)\sigma_i\,dz, (i = x, y, xy) \quad \text{and} \quad Q_i = \int_{-h/2}^{h/2} g\sigma_i\,dz, (i = xz, yz)
\tag{12}
$$

The variation of potential energy of the applied loads can be expressed as

$$\delta V = -\int_A q\,\delta u_3\,dA + \int_A\left(N_x^0\,\frac{\partial u_3}{\partial x}\frac{\partial \delta u_3}{\partial x} + N_y^0\,\frac{\partial u_3}{\partial y}\frac{\partial \delta u_3}{\partial y} + 2N_{xy}^0\,\frac{\partial u_3}{\partial x}\frac{\partial \delta u_3}{\partial y}\right)dA \qquad (13)$$

where q and $\left(N_x^0, N_y^0, N_{xy}^0\right)$ are transverse and in-plane applied loads, respectively.

The variation of kinetic energy of the plate can be written as

$$
\begin{aligned}
\delta K &= \int_V \left(\dot{u}_1\,\delta\dot{u}_1 + \dot{u}_2\,\delta\dot{u}_2 + \dot{u}_3\,\delta\dot{u}_3\right)\rho(z)\,dA\,dz \\
&= \int_A \Big\{ I_0\left[\dot{u}\,\delta\dot{u} + \dot{v}\,\delta\dot{v} + \left(\dot{w}_b + \dot{w}_s\right)\delta\left(\dot{w}_b + \dot{w}_s\right)\right] \\
&\quad - I_1\left(\dot{u}\,\frac{\partial \delta\dot{w}_b}{\partial x} + \frac{\partial \dot{w}_b}{\partial x}\,\delta\dot{u} + \dot{v}\,\frac{\partial \delta\dot{w}_b}{\partial y} + \frac{\partial \dot{w}_b}{\partial y}\,\delta\dot{v}\right) \\
&\quad - J_1\left(\dot{u}\,\frac{\partial \delta\dot{w}_s}{\partial x} + \frac{\partial \dot{w}_s}{\partial x}\,\delta\dot{u} + \dot{v}\,\frac{\partial \delta\dot{w}_s}{\partial y} + \frac{\partial \dot{w}_s}{\partial y}\,\delta\dot{v}\right) \\
&\quad + I_2\left(\frac{\partial \dot{w}_b}{\partial x}\frac{\partial \delta\dot{w}_b}{\partial x} + \frac{\partial \dot{w}_b}{\partial y}\frac{\partial \delta\dot{w}_b}{\partial y}\right) + K_2\left(\frac{\partial \dot{w}_s}{\partial x}\frac{\partial \delta\dot{w}_s}{\partial x} + \frac{\partial \dot{w}_s}{\partial y}\frac{\partial \delta\dot{w}_s}{\partial y}\right) \\
&\quad + J_2\left(\frac{\partial \dot{w}_b}{\partial x}\frac{\partial \delta\dot{w}_s}{\partial x} + \frac{\partial \dot{w}_s}{\partial x}\frac{\partial \delta\dot{w}_b}{\partial x} + \frac{\partial \dot{w}_b}{\partial y}\frac{\partial \delta\dot{w}_s}{\partial y} + \frac{\partial \dot{w}_s}{\partial y}\frac{\partial \delta\dot{w}_b}{\partial y}\right) \Big\}\,dA
\end{aligned}
\qquad (14)
$$

where dot-superscript convention indicates the differentiation with respect to the time variable t; $\rho(z)$ is the mass density; and $\left(I_0, I_1, J_1, I_2, J_2, K_2\right)$ are mass inertias defined as

$$\left(I_0, I_1, J_1, I_2, J_2, K_2\right) = \int_{-h/2}^{h/2}\left(1, z, f, z^2, zf, f^2\right)\rho(z)\,dz \qquad (15)$$

Substituting the expressions for δU, δV, and δK from Eqs. (11), (13), and (14) into Eq. (10) and integrating by parts, and collecting the coefficients of δu, δv, δw_b, and δw_s, the following equations of motion of the plate are obtained

$$\delta u: \quad \frac{\partial N_x}{\partial x} + \frac{\partial N_{xy}}{\partial y} = I_0\ddot{u} - I_1\frac{\partial \ddot{w}_b}{\partial x} - J_1\frac{\partial \ddot{w}_s}{\partial x} \qquad (16a)$$

$$\delta v: \quad \frac{\partial N_{xy}}{\partial x} + \frac{\partial N_y}{\partial y} = I_0\ddot{v} - I_1\frac{\partial \ddot{w}_b}{\partial y} - J_1\frac{\partial \ddot{w}_s}{\partial y} \qquad (16b)$$

$$\mathrm{u}\, w_b : \frac{\partial^2 M_x^b}{\partial x^2} + 2\frac{\partial^2 M_{xy}^b}{\partial x \partial y} + \frac{\partial^2 M_y^b}{\partial y^2} + q + \tilde{N}$$

$$= I_0 \left(\ddot{w}_b + \ddot{w}_s \right) + I_1 \left(\frac{\partial \ddot{u}}{\partial x} + \frac{\partial \ddot{v}}{\partial y} \right) - I_2 \nabla^2 \ddot{w}_b - J_2 \nabla^2 \ddot{w}_s \qquad (16c)$$

$$\mathrm{u}\, w_s : \frac{\partial^2 M_x^s}{\partial x^2} + 2\frac{\partial^2 M_{xy}^s}{\partial x \partial y} + \frac{\partial^2 M_y^s}{\partial y^2} + \frac{\partial Q_{xz}}{\partial x} + \frac{\partial Q_{yz}}{\partial y} + q + \tilde{N}$$

$$= I_0 \left(\ddot{w}_b + \ddot{w}_s \right) + J_1 \left(\frac{\partial \ddot{u}}{\partial x} + \frac{\partial \ddot{v}}{\partial y} \right) - J_2 \nabla^2 \ddot{w}_b - K_2 \nabla^2 \ddot{w}_s \qquad (16d)$$

where

$$\tilde{N} = N_x^0 \frac{\partial^2 \left(w_b + w_s \right)}{\partial x^2} + N_y^0 \frac{\partial^2 \left(w_b + w_s \right)}{\partial y^2} + 2N_{xy}^0 \frac{\partial^2 \left(w_b + w_s \right)}{\partial x \partial y} \qquad (17)$$

The boundary conditions of present theory involve specifying the six following pairs:

$$
\begin{array}{ccc}
u_n & \text{or} & N_{nn} \\
u_s & \text{or} & N_{ns} \\
\partial w_b / \partial n & \text{or} & M_{nn}^b \\
\partial w_s / \partial n & \text{or} & M_{nn}^s \\
w_b & \text{or} & V_n^b \\
w_s & \text{or} & V_n^s
\end{array} \qquad (18)
$$

where

$$u_n = u n_x + v n_y, \ u_s = -u n_y + v n_x$$

$$N_{nn} = N_x n_x^2 + N_y n_y^2 + 2 N_{xy} n_x n_y, \ N_{ns} = \left(N_y - N_x \right) n_x n_y + N_{xy} \left(n_x^2 - n_y^2 \right)$$

$$M_{nn}^b = M_x^b n_x^2 + M_y^b n_y^2 + 2 M_{xy}^b n_x n_y, \ M_{nn}^s = M_x^s n_x^2 + M_y^s n_y^2 + 2 M_{xy}^s n_x n_y$$

$$V_n^b = Q_x^b n_x + Q_y^b n_y + \frac{\partial M_{ns}^b}{\partial s}, \ V_n^s = Q_x^s n_x + Q_y^s n_y + \frac{\partial M_{ns}^s}{\partial s}$$

$$Q_x^b = \frac{\partial M_x^b}{\partial x} + \frac{\partial M_{xy}^b}{\partial y} + N_x^0 \frac{\partial \left(w_b + w_s \right)}{\partial x} + N_{xy}^0 \frac{\partial \left(w_b + w_s \right)}{\partial y} - I_1 \ddot{u} + I_2 \frac{\partial \ddot{w}_b}{\partial x} + J_2 \frac{\partial \ddot{w}_s}{\partial x}$$

$$Q_y^b = \frac{\partial M_y^b}{\partial y} + \frac{\partial M_{xy}^b}{\partial x} + N_{xy}^0 \frac{\partial \left(w_b + w_s \right)}{\partial x} + N_y^0 \frac{\partial \left(w_b + w_s \right)}{\partial y} - I_1 \ddot{v} + I_2 \frac{\partial \ddot{w}_b}{\partial y} + J_2 \frac{\partial \ddot{w}_s}{\partial y}$$

(19)

$$Q_x^s = \frac{\partial M_x^s}{\partial x} + \frac{\partial M_{xy}^s}{\partial y} + Q_{xz} + N_x^0 \frac{\partial \left(w_b + w_s \right)}{\partial x} + N_{xy}^0 \frac{\partial \left(w_b + w_s \right)}{\partial y} - J_1 \ddot{u} + J_2 \frac{\partial \ddot{w}_b}{\partial x} + K_2 \frac{\partial \ddot{w}_s}{\partial x}$$

$$Q_y^s = \frac{\partial M_y^s}{\partial y} + \frac{\partial M_{xy}^s}{\partial x} + Q_{yz} + N_{xy}^0 \frac{\partial \left(w_b + w_s \right)}{\partial x} + N_y^0 \frac{\partial \left(w_b + w_s \right)}{\partial y} - J_1 \ddot{v} + J_2 \frac{\partial \ddot{w}_b}{\partial y} + K_2 \frac{\partial \ddot{w}_s}{\partial y}$$

$$M_{ns}^b = \left(M_y^b - M_x^b \right) n_x n_y + M_{xy}^b \left(n_x^2 - n_y^2 \right), \ M_{ns}^s = \left(M_y^s - M_x^s \right) n_x n_y + M_{xy}^s \left(n_x^2 - n_y^2 \right)$$

By substituting Eq. (6) into Eq. (9) and the subsequent results into Eq. (12), the stress resultants are obtained as

$$\begin{Bmatrix} \{N\} \\ \{M^b\} \\ \{M^s\} \end{Bmatrix} = \begin{bmatrix} [A] & [B] & [B^s] \\ [B] & [D] & [D^s] \\ [B^s] & [D^s] & [H^s] \end{bmatrix} \begin{Bmatrix} \{v^0\} \\ \{|^b\} \\ \{|^s\} \end{Bmatrix} \quad \text{and} \quad \{Q\} = \left[A^s \right] \{x^s\} \tag{20}$$

where

$$\left([A], [B], \left[B^s \right], [D], \left[D^s \right], \left[H^s \right] \right) = \begin{bmatrix} 1 & \text{\text€} & 0 \\ \text{\text€} & 1 & 0 \\ 0 & 0 & (1-\text{\text€})/2 \end{bmatrix} \left(A, B, B^s, D, D^s, H^s \right) \tag{21a}$$

$$\left(A, B, B^s, D, D^s, H^s \right) = \int_{-h/2}^{h/2} \left(1, z, f, z^2, zf, f^2 \right) \frac{E(z)}{1-\text{\text€}^2} dz \tag{21b}$$

$$\left[A^s \right] = \begin{bmatrix} 1 & 0 \\ 0 & 1 \end{bmatrix} A^s, \ A^s = \int_{-h/2}^{h/2} \frac{E(z)}{2(1+\text{\text€})} g^2 dz \tag{21c}$$

By substituting Eq. (20) into Eq. (16), the equations of motion can be expressed in terms of displacements $\left(u, v, w_b, w_s \right)$ as

9

$$A\left(\frac{\partial^2 u}{\partial x^2} + \frac{1-\epsilon}{2}\frac{\partial^2 u}{\partial y^2} + \frac{1+\epsilon}{2}\frac{\partial^2 v}{\partial x \partial y}\right) - B\nabla^2\frac{\partial w_b}{\partial x} - B^s\nabla^2\frac{\partial w_s}{\partial x} = I_0\ddot{u} - I_1\frac{\partial \ddot{w}_b}{\partial x} - J_1\frac{\partial \ddot{w}_s}{\partial x} \quad (22\text{a})$$

$$A\left(\frac{\partial^2 v}{\partial y^2} + \frac{1-\epsilon}{2}\frac{\partial^2 v}{\partial x^2} + \frac{1+\epsilon}{2}\frac{\partial^2 u}{\partial x \partial y}\right) - B\nabla^2\frac{\partial w_b}{\partial y} - B^s\nabla^2\frac{\partial w_s}{\partial y} = I_0\ddot{v} - I_1\frac{\partial \ddot{w}_b}{\partial y} - J_1\frac{\partial \ddot{w}_s}{\partial y} \quad (22\text{b})$$

$$B\nabla^2\left(\frac{\partial u}{\partial x} + \frac{\partial v}{\partial y}\right) - D\nabla^4 w_b - D^s\nabla^4 w_s + q + \tilde{N}$$
$$= I_0\left(\ddot{w}_b + \ddot{w}_s\right) + I_1\left(\frac{\partial \ddot{u}}{\partial x} + \frac{\partial \ddot{v}}{\partial y}\right) - I_2\nabla^2\ddot{w}_b - J_2\nabla^2\ddot{w}_s$$
$$(22\text{c})$$

$$B^s\nabla^2\left(\frac{\partial u}{\partial x} + \frac{\partial v}{\partial y}\right) - D^s\nabla^4 w_b - H^s\nabla^4 w_s + A^s\nabla^2 w_s + q + \tilde{N}$$
$$= I_0\left(\ddot{w}_b + \ddot{w}_s\right) + J_1\left(\frac{\partial \ddot{u}}{\partial x} + \frac{\partial \ddot{v}}{\partial y}\right) - J_2\nabla^2\ddot{w}_b - K_2\nabla^2\ddot{w}_s$$
$$(22\text{d})$$

Clearly, when the effect of transverse shear deformation is neglected ($w_s = 0$), Eq. (22) yields the equations of motion of FG plate based on the classical plate theory.

3. Closed-form solution for the simply supported rectangular plate

Consider a simply supported rectangular plate with length a and width b under transverse load q and in-plane forces in two directions ($N_x^0 = x_1 N_{cr}, N_y^0 = x_2 N_{cr}, N_{xy}^0 = 0$). Based on the Navier approach, the following expansions of displacements are chosen to automatically satisfy the simply supported boundary conditions of plate

$$u(x,y,t) = \sum_{m=1}^{\infty}\sum_{n=1}^{\infty} U_{mn} e^{i\check{S}t} \cos r x \sin s y$$
$$v(x,y,t) = \sum_{m=1}^{\infty}\sum_{n=1}^{\infty} V_{mn} e^{i\check{S}t} \sin r x \cos s y$$
$$w_b(x,y,t) = \sum_{m=1}^{\infty}\sum_{n=1}^{\infty} W_{bmn} e^{i\check{S}t} \sin r x \sin s y$$
$$w_s(x,y,t) = \sum_{m=1}^{\infty}\sum_{n=1}^{\infty} W_{smn} e^{i\check{S}t} \sin r x \sin s y$$
$$(23)$$

where $i = \sqrt{-1}$, $r = mf/a$, $s = nf/b$, $\left(U_{mn}, V_{mn}, W_{bmn}, W_{smn}\right)$ are coefficients, and

$\bar{S}$ is the frequency of vibration. The transverse load q is also expanded in the double-Fourier sine series as

$$q(x,y) = \sum_{m=1}^{\infty} \sum_{n=1}^{\infty} Q_{mn} \sin r x \sin s y \qquad (24)$$

where

$$Q_{mn} = \frac{4}{ab} \int_0^a \int_0^b q(x,y) \sin r x \sin s\, y\, dx dy = \begin{cases} q_0 & \text{for sinusoidally distributed load} \\ \dfrac{16 q_0}{mn f^2} & \text{for uniformly distributed load} \end{cases} \qquad (25)$$

Substituting Eq. (23) into Eq. (22), the closed-form solutions can be obtained from

$$\left(\begin{bmatrix} s_{11} & s_{12} & s_{13} & s_{14} \\ s_{12} & s_{22} & s_{23} & s_{24} \\ s_{13} & s_{23} & s_{33}+k & s_{34}+k \\ s_{14} & s_{24} & s_{34}+k & s_{44}+k \end{bmatrix} - \bar{S}^2 \begin{bmatrix} m_{11} & 0 & m_{13} & m_{14} \\ 0 & m_{22} & m_{23} & m_{24} \\ m_{13} & m_{23} & m_{33} & m_{34} \\ m_{14} & m_{24} & m_{34} & m_{44} \end{bmatrix} \right) \begin{Bmatrix} U_{mn} \\ V_{mn} \\ W_{bmn} \\ W_{smn} \end{Bmatrix} = \begin{Bmatrix} 0 \\ 0 \\ Q_{mn} \\ Q_{mn} \end{Bmatrix} \qquad (26)$$

where

$$s_{11} = A r^2 + \frac{1-\epsilon}{2} A s^2,\ s_{12} = \frac{1+\epsilon}{2} A r s,\ s_{22} = \frac{1-\epsilon}{2} A r^2 + A s^2$$

$$s_{13} = -B r (r^2 + s^2),\ s_{14} = -B^s r (r^2 + s^2),\ s_{23} = -B s (r^2 + s^2)$$

$$s_{24} = -B^s s (r^2 + s^2),\ s_{33} = D(r^2 + s^2)^2,\ s_{34} = D^s (r^2 + s^2)^2 \qquad (27)$$

$$s_{44} = H^s (r^2 + s^2)^2 + A^s (r^2 + s^2),\ k = N_{cr}(x_1 r^2 + x_2 s^2)$$

$$m_{11} = m_{22} = I_0,\ m_{13} = -r I_1,\ m_{14} = -r J_1,\ m_{23} = -s I_1,\ m_{24} = -s J_1$$

$$m_{33} = I_0 + I_2 (r^2 + s^2),\ m_{34} = I_0 + J_2 (r^2 + s^2),\ m_{44} = I_0 + K_2 (r^2 + s^2)$$

4. Results and discussion

In this section, various numerical examples are presented and discussed to verify the accuracy of present theory in predicting the bending, buckling, and vibration responses of simply supported FG plates. For numerical results, an Al/Al$_2$O$_3$ plate composed of aluminum (as metal) and alumina (as ceramic) is considered. The Young's modulus and density of aluminum are $E_m = 70\,\text{GPa}$ and $\rho_m = 2702\,\text{kg/m}^3$, respectively, and those of

alumina are $E_c = 380\,\text{GPa}$ and $\rho_c = 3800\,\text{kg/m}^3$, respectively. For verification purpose, the obtained results are compared with those predicted using various plate theories. The description of various displacement models is given in Table 1. In all examples, a shear correction factor of 5/6 is used for FSDT and the rotary inertias are included in all theories. The Poisson's ratio of the plate is assumed to be constant through the thickness and equal to 0.3. For convenience, the following nondimensionalizations are used in presenting the numerical results in graphical and tabular form:

$$\bar{w} = \frac{10 E_c h^3}{q_0 a^4} w\left(\frac{a}{2}, \frac{b}{2}\right), \bar{\sigma}_x = \frac{h}{q_0 a} \sigma_x\left(\frac{a}{2}, \frac{b}{2}, \frac{h}{2}\right), \bar{\sigma}_y = \frac{h}{q_0 a} \sigma_y\left(\frac{a}{2}, \frac{b}{2}, \frac{h}{3}\right), D = \frac{E h^3}{12\left(1 - \nu^2\right)}$$

$$\bar{\sigma}_{xy} = \frac{h}{q_0 a} \sigma_{xy}\left(0, 0, -\frac{h}{3}\right), \hat{N} = \frac{N_{cr} b^2}{\pi^2 D}, \bar{N} = \frac{N a^2}{E_m h^3}, \check{S} = \check{S} h \sqrt{\rho_c / E_c}, \check{S} = \check{S} \frac{a^2}{h} \sqrt{\rho_c / E_c}$$ (28)

4.1. Bending problem

Example 1: The first example is carried out for square plate subjected to uniformly distributed load ($a = 10h$). Table 2 shows the comparison of nondimensional deflections and stresses obtained by present theory with those given by Zenkour [16] based on sinusoidal shear deformation theory (SSDT). It can be seen that the proposed new SSDT and conventional SSDT [16] give identical results of deflections as well as stresses for all values of power law index p. It should be noted that the proposed new SSDT involves four unknowns as against five in case of conventional SSDT [16]. It is observed that the stresses for a fully ceramic plate are the same as those for a fully metal plate. This is due to the fact that the plate for these two cases is fully homogenous and the nondimensional stresses do not depend on the value of the elastic modulus.

Example 2: Table 3 shows the comparison of nondimensional deflections and stresses of square plate subjected to sinusoidally distributed load ($a = 10h$). The obtained results are compared with those given by Benyoucef et al. [23] based on the hyperbolic shear

deformation theory (HSDT). It can be seen that an excellent agreement is obtained for all values of power law index p.

To illustrate the accuracy of present theory for wide range of power law index p and thickness ratio a/h, the variations of nondimensional deflection $\bar{w}$ with respect to power law index p and thickness ratio a/h are illustrated in Fig. 1 and Fig. 2, respectively, for square plate subjected to sinusoidally distributed load. The obtained results are compared with those predicted by CPT and TSDT [12]. It can be seen that the results of present theory and TSDT are almost identical, and the CPT underestimates the deflection of plate. Since the transverse shear deformation effects are not considered in CPT, the values of nondimensional deflection $\bar{w}$ predicted by CPT are independent of thickness ratio a/h (see Fig. 2).

4.2. Buckling problem

Due to the variation of material properties through the thickness, the stretching-bending coupling exists in FG plate. This coupling produces deflection and bending moments when plate is subjected to in-plane compressive loads. Hence, bifurcation-type buckling will not occur [34-35]. The conditions for bifurcation-type buckling to occur under the action of in-plane loads are examined by Aydogdu [36] and Naderi and Saidi [37]. It is observed that the bifurcation-type buckling occurs when the plate is fully clamped. For movable-edge plate, the bifurcation-type buckling occurs when the in-plane loads are applied at the neutral surface. Therefore, the buckling analysis is presented herein for FG plate subjected to in-plane loads acting on the neutral surface.

Example 3: Since the buckling results of FG plate are not available in the literature, only isotropic plate is used herein for verification. Table 4 shows the nondimensional buckling loads $\hat{N}$ of isotropic plate ($p = 0$) subjected to different loading types for

13

different values of aspect ratio a/b and thickness ratio h/b. The obtained results are compared with those of Shufrin and Eisenberger [38] based on FSDT and TSDT. A good agreement is found for all cases ranging from moderately thick to very thick plates. The variations of nondimensional critical buckling load $\bar{N}$ with respect to power law index p and thickness ratio a/h are illustrated in Fig. 3 and Fig. 4, respectively, for square plate under biaxial compression. It is observed that the proposed theory and TSDT give almost identical results, and CPT overestimates the buckling loads of plate due to ignoring transverse shear deformation effects. The difference between CPT and shear deformation theories (TSDT and present theory) decreases when the thickness ratio a/h increases (see Fig. 4).

4.3. Free vibration problem

Example 4: Nondimensional fundamental frequencies $\check{S}$ of square plate for different values of thickness ratio h/a and power law index p are presented in Table 5. The obtained results are compared with those reported by and Hosseini-Hashemi et al. [11] based on FSDT and and Hosseini-Hashemi et al. [39] based on TSDT. It is observed that there is an excellent agreement between the results predicted by present theory, FSDT [11], and TSDT [39].

Example 5: To verify the higher order modes of vibration, the first four nondimensional frequencies $\check{S}$ are compared in Table 6 for rectangular plate ($b = 2a$) with thickness ratio varied from 5 to 20 and power law index varied from 0 to 10. The nondimensional frequencies obtained by using proposed theory and TSDT [12] are compared with those given by Hosseini-Hashemi et al. [11] based on FSDT. It can be seen that the results predicted by proposed theory and TSDT are almost identical for all modes of vibration of thin to thick plates. Also, the proposed theory gives more accurate prediction of

natural frequency compared to FSDT. The maximum difference between present theory and TSDT is 0.1% at the fourth mode ($a/h = 5$, $p = 5$), while the maximum difference between FSDT and TSDT is 5.64% at the fourth mode ($a/h = 5$, $p = 10$). However, this difference decreases at lower modes of vibration. For example, the differences between FSDT and TSDT are 1.26%, 1.78%, 2.44%, and 5.64% at the first, second, third, and fourth modes ($a/h = 5$, $p = 10$), respectively.

The variations of nondimensional fundamental frequency $\check{S}$ of square plate with respect to power law index p and thickness ratio a/h are compared in Fig. 5 and Fig. 6, respectively. It is observed that the nondimensional frequencies $\check{S}$ predicted by present theory and TSDT are almost identical, and the CPT overestimates the frequency of thick plate.

5. Conclusions

A new sinusoidal shear deformation theory is developed for bending, buckling, and vibration of FG plates. Unlike the conventional sinusoidal shear deformation theory, the proposed sinusoidal shear deformation theory contains only four unknowns and has strong similarities with the CPT in many aspects such as equations of motion, boundary conditions, and stress resultant expressions. Equations of motion are derived from the Hamilton's principle. Closed-form solutions are obtained for simply supported plates. The accuracy of the proposed theory has been verified for the bending, buckling, and free vibration analyses of FG plates. All comparison studies show that the deflection, stress, buckling load, and natural frequency obtained by the proposed theory with four unknowns are almost identical with those predicted by other shear deformation theories containing five unknowns. The practical utilities of this theory are: (1) there is no need to use a shear correction factor; (2) the finite element model based on this theory will be

15

free from shear locking since the CPT comes out as a special case of the present theory; and (3) the theory is simple and time efficient due to involving only four unknowns. In conclusion, it can be said that the proposed theory is accurate and efficient in predicting the bending, buckling, and vibration responses of FG plates.

References

[1] Javaheri R, Eslami MR. Buckling of functionally graded plates under in-plane compressive loading. Journal of Applied Mathematics and Mechanics 2002;82(4):277-283.

[2] Zhang DG, Zhou YH. A theoretical analysis of FGM thin plates based on physical neutral surface. Computational Materials Science 2008;44(2):716-720.

[3] Mohammadi M, Saidi AR, Jomehzadeh E. Levy solution for buckling analysis of functionally graded rectangular plates. Applied Composite Materials 2010;17(2):81-93.

[4] Bodaghi M, Saidi AR. Stability analysis of functionally graded rectangular plates under nonlinearly varying in-plane loading resting on elastic foundation. Archive of Applied Mechanics 2011;81(6):765-780.

[5] Della Croce L, Venini P. Finite elements for functionally graded Reissner–Mindlin plates. Computer Methods in Applied Mechanics and Engineering 2004;193(9-11):705-725.

[6] Ganapathi M, Prakash T, Sundararajan N. Influence of functionally graded material on buckling of skew plates under mechanical loads. Journal of Engineering Mechanics 2006;132(8):902-905.

[7] Zhao X, Liew KM. Geometrically nonlinear analysis of functionally graded plates using the element-free kp-Ritz method. Computer Methods in Applied Mechanics

and Engineering 2009;198(33-36):2796-2811.

[8] Zhao X, Lee YY, Liew KM. Free vibration analysis of functionally graded plates using the element-free kp-Ritz method. Journal of Sound and Vibration 2009;319(3-5):918-939.

[9] Lee YY, Zhao X, Reddy JN. Postbuckling analysis of functionally graded plates subject to compressive and thermal loads. Computer Methods in Applied Mechanics and Engineering 2010;199(25-28):1645-1653.

[10] Hosseini-Hashemi S, Rokni Damavandi Taher H, Akhavan H, Omidi M. Free vibration of functionally graded rectangular plates using first-order shear deformation plate theory. Applied Mathematical Modelling 2010;34(5):1276-1291.

[11] Hosseini-Hashemi S, Fadaee M, Atashipour SR. A new exact analytical approach for free vibration of Reissner-Mindlin functionally graded rectangular plates. International Journal of Mechanical Sciences 2011;53(1):11-22.

[12] Reddy JN. Analysis of functionally graded plates. International Journal for Numerical Methods in Engineering 2000;47(1-3):663-684.

[13] Karama M, Afaq KS, Mistou S. Mechanical behaviour of laminated composite beam by the new multi-layered laminated composite structures model with transverse shear stress continuity. International Journal of Solids and Structures 2003;40(6):1525-1546.

[14] Zenkour AM. A comprehensive analysis of functionally graded sandwich plates: Part 1-Deflection and stresses. International Journal of Solids and Structures 2005;42(18-19):5224-5242.

[15] Zenkour AM. A comprehensive analysis of functionally graded sandwich plates: Part 2-Buckling and free vibration. International Journal of Solids and Structures

2005;42(18-19):5243-5258.

[16] Zenkour AM. Generalized shear deformation theory for bending analysis of functionally graded plates. Applied Mathematical Modelling 2006;30(1):67-84.

[17] Xiao JR, Batra RC, Gilhooley DF, Gillespie Jr JW, McCarthy MA. Analysis of thick plates by using a higher-order shear and normal deformable plate theory and MLPG method with radial basis functions. Computer Methods in Applied Mechanics and Engineering 2007;196(4-6):979-987.

[18] Matsunaga H. Free vibration and stability of functionally graded plates according to a 2-D higher-order deformation theory. Composite Structures 2008;82(4):499-512.

[19] Pradyumna S, Bandyopadhyay JN. Free vibration analysis of functionally graded curved panels using a higher-order finite element formulation. Journal of Sound and Vibration 2008;318(1-2):176-192.

[20] Fares ME, Elmarghany MK, Atta D. An efficient and simple refined theory for bending and vibration of functionally graded plates. Composite Structures 2009;91(3):296-305.

[21] Talha M, Singh BN. Static response and free vibration analysis of FGM plates using higher order shear deformation theory. Applied Mathematical Modelling 2010;34(12):3991-4011.

[22] Talha M, Singh BN. Thermo-mechanical buckling analysis of finite element modelled functionally graded ceramic-metal plates. International Journal of Applied 2011;3(4):867-880.

[23] Benyoucef S, Mechab I, Tounsi A, Fekrar A, Ait Atmane H, Adda Bedia EA. Bending of thick functionally graded plates resting on Winkler–Pasternak elastic

18

foundations. Mechanics of Composite Materials 2010;46(4):425-434.

[24] Atmane HA, Tounsi A, Mechab I, Adda Bedia EA. Free vibration analysis of functionally graded plates resting on Winkler–Pasternak elastic foundations using a new shear deformation theory. International Journal of Mechanics and Materials in Design 2010;6(2):113-121.

[25] Meiche NE, Tounsi A, Ziane N, Mechab I, Adda.Bedia EA. A new hyperbolic shear deformation theory for buckling and vibration of functionally graded sandwich plate. International Journal of Mechanical Sciences 2011;53(4):237-247.

[26] Mantari JL, Oktem AS, Guedes Soares C. Bending response of functionally graded plates by using a new higher order shear deformation theory. Composite Structures 2012;94(2):714-723.

[27] Xiang S, Jin Y-x, Bi Z-y, Jiang S-x, Yang M-s. A n-order shear deformation theory for free vibration of functionally graded and composite sandwich plates. Composite Structures 2011;93(11):2826-2832.

[28] Merdaci S, Tounsi A, Houari M, Mechab I, Hebali H, Benyoucef S. Two new refined shear displacement models for functionally graded sandwich plates. Archive of Applied Mechanics 2011;81(11):1507-1522.

[29] Ameur M, Tounsi A, Mechab I, El Bedia AA. A new trigonometric shear deformation theory for bending analysis of functionally graded plates resting on elastic foundations. KSCE Journal of Civil Engineering 2011;15(8):1405-1414.

[30] Tounsi A, Houari MSA, Benyoucef S, Adda Bedia EA. A refined trigonometric shear deformation theory for thermoelastic bending of functionally graded sandwich plates. Aerospace Science and Technology 2011; doi: 10.1016/j.ast.2011.11.009.

[31] Yang J, Liew KM, Kitipornchai S. Stochastic analysis of compositionally graded plates with system randomness under static loading. International Journal of Mechanical Sciences 2005;47(10):1519-1541.

[32] Kitipornchai S, Yang J, Liew KM. Random vibration of the functionally graded laminates in thermal environments. Computer Methods in Applied Mechanics and Engineering 2006;195(9-12):1075-1095.

[33] Reddy JN. Energy principles and variational methods in applied mechanics: John Wiley & Sons Inc; 2002.

[34] Liew KM, Yang J, Kitipornchai S. Postbuckling of piezoelectric FGM plates subject to thermo-electro-mechanical loading. International Journal of Solids and Structures 2003;40(15):3869-3892.

[35] Qatu MS, Leissa AW. Buckling or transverse deflections of unsymmetrically laminated plates subjected to in-plane loads. AIAA Journal 1993;31(1):189-194.

[36] Aydogdu M. Conditions for functionally graded plates to remain flat under in-plane loads by classical plate theory. Composite Structures 2008;82(1):155-157.

[37] Naderi A, Saidi AR. On pre-buckling configuration of functionally graded Mindlin rectangular plates. Mechanics Research Communications 2010;37(6):535-538.

[38] Shufrin I, Eisenberger M. Stability and vibration of shear deformable plates-first order and higher order analyses. International Journal of Solids and Structures 2005;42(3-4):1225-1251.

[39] Hosseini-Hashemi S, Fadaee M, Atashipour SR. Study on the free vibration of thick functionally graded rectangular plates according to a new exact closed-form procedure. Composite Structures 2011;93(2):722-735.

Figure Captions

Fig. 1. Comparison of the variation of nondimensional deflection $\bar{w}$ of square plate under sinusoidally distributed load versus power law index p ($a = 5h$)

Fig. 2. Comparison of the variation of nondimensional deflection $\bar{w}$ of square plate under sinusoidally distributed load versus thickness ratio a/h

Fig. 3. Comparison of the variation of nondimensional critical buckling load $\bar{N}$ of square plate under biaxial compression versus power law index p ($a = 5h$)

Fig. 4. Comparison of the variation of nondimensional critical buckling load $\bar{N}$ of square plate under biaxial compression versus thickness ratio a/h

Fig. 5. Comparison of the variation of nondimensional fundamental frequency $\check{S}$ of square plate versus power law index p ($a = 5h$)

Fig. 6. Comparison of the variation of nondimensional fundamental frequency $\check{S}$ of square plate versus thickness ratio a/h

Table Captions

Table 1. Displacement models

Table 2. Comparison of nondimensional deflection and stresses of square plate under uniformly distributed load ($m, n = 100$ term series, $a = 10h$)

Table 3. Comparison of nondimensional deflection and stresses of square plate under sinusoidally distributed load ($a = 10h$)

Table 4. Comparison of nondimensional critical buckling load $\hat{N}$ of isotropic plate under different loading types ($p = 0$)

Table 5. Comparison of nondimensional fundamental frequency $\check{S}$ of square plate

Table 6. Comparison of the first four nondimensional frequency $\check{S}$ of rectangular plate ($b = 2a$)

Fig. 1. Comparison of the variation of nondimensional deflection $\bar{w}$ of square plate under sinusoidally distributed load versus power law index p ($a = 5h$)

Fig. 2. Comparison of the variation of nondimensional deflection $\bar{w}$ of square plate under sinusoidally distributed load versus thickness ratio a/h

Fig. 3. Comparison of the variation of nondimensional critical buckling load $\bar{N}$ of square plate under biaxial compression versus power law index p ($a = 5h$)

Fig. 4. Comparison of the variation of nondimensional critical buckling load $\bar{N}$ of square plate under biaxial compression versus thickness ratio a / h

Fig. 5. Comparison of the variation of nondimensional fundamental frequency $\check{S}$ of square plate versus power law index p ($a = 5h$)

Fig. 6. Comparison of the variation of nondimensional fundamental frequency $\check{S}$ of square plate versus thickness ratio a/h

Table 1. Displacement models

Model	Theory	Unknowns
CPT	Classical plate theory	3
FSDT	First-order shear deformation theory	5
TSDT	Third-order shear deformation theory	5
HSDT	Hyperbolic shear deformation theory	5
SSDT	Sinusoidal shear deformation theory	5
Present	New sinusoidal shear deformation theory	4

Table 2. Comparison of nondimensional deflection and stresses of square plate under uniformly distributed load ($m, n = 100$ term series, $a = 10h$)

p	Method	$\bar{w}$	$\bar{\sigma}_x$	$\bar{\sigma}_y$	$\bar{\tau}_{xy}$	$\bar{\tau}_{yz}$	$\bar{\tau}_{xz}$
Ceramic	SSDT [16]	0.4665	2.8932	1.9103	1.2850	0.4429	0.5114
	Present	0.4665	2.8932	1.9103	1.2850	0.4429	0.5114
1	SSDT [16]	0.9287	4.4745	2.1962	1.1143	0.5446	0.5114
	Present	0.9287	4.4745	2.1692	1.1143	0.5446	0.5114
2	SSDT [16]	1.1940	5.2296	2.0338	0.9907	0.5734	0.4700
	Present	1.1940	5.2296	2.0338	0.9907	0.5734	0.4700
3	SSDT [16]	1.3200	5.6108	1.8593	1.0047	0.5629	0.4367
	Present	1.3200	5.6108	1.8593	1.0047	0.5629	0.4367
4	SSDT [16]	1.3890	5.8915	1.7197	1.0298	0.5346	0.4204
	Present	1.3890	5.8915	1.7197	1.0298	0.5346	0.4204
5	SSDT [16]	1.4356	6.1504	1.6104	1.0451	0.5031	0.4177
	Present	1.4356	6.1504	1.6104	1.0451	0.5031	0.4177
6	SSDT [16]	1.4727	6.4043	1.5214	1.0536	0.4755	0.4227
	Present	1.4727	6.4043	1.5214	1.0536	0.4755	0.4227
7	SSDT [16]	1.5049	6.6547	1.4467	1.0589	0.4543	0.4310
	Present	1.5049	6.6547	1.4467	1.0589	0.4543	0.4310
8	SSDT [16]	1.5343	6.8999	1.3829	1.0628	0.4392	0.4399
	Present	1.5343	6.8999	1.3829	1.0628	0.4392	0.4399
9	SSDT [16]	1.5617	7.1383	1.3283	1.0620	0.4291	0.4481
	Present	1.5617	7.1383	1.3283	1.0662	0.4291	0.4481
10	SSDT [16]	1.5876	7.3689	1.2820	1.0694	0.4227	0.4552
	Present	1.5876	7.3689	1.2820	1.0694	0.4227	0.4552
Metal	SSDT [16]	2.5327	2.8932	1.9103	1.2850	0.4429	0.5114
	Present	2.5327	2.8932	1.9103	1.2850	0.4429	0.5114

Table 3. Comparison of nondimensional deflection and stresses of square plate under sinusoidally distributed load ($a = 10h$)

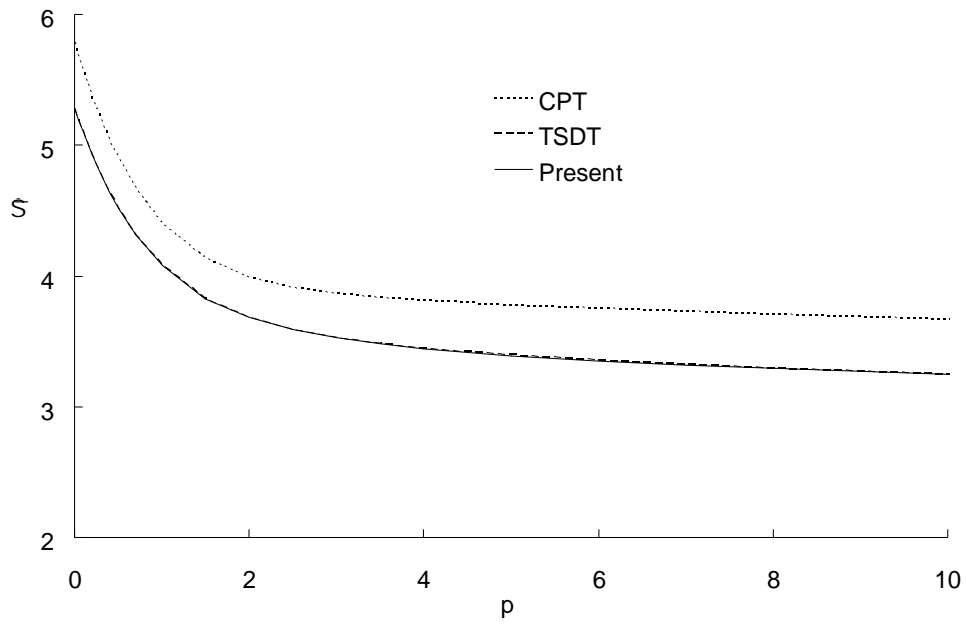| p	Method	$\bar{w}$	$\bar{\sigma}_x$	$\bar{\sigma}_y$	$\bar{\sigma}_{xy}$	$\bar{\sigma}_{yz}$	$\bar{\sigma}_{xz}$
Ceramic	HSDT [23]	0.2960	1.9955	1.3121	0.7065	0.2132	0.2462
	Present	0.2960	1.9955	1.3121	0.7065	0.2132	0.2462
1	HSDT [23]	0.5889	3.0870	1.4894	0.6110	0.2622	0.2462
	Present	0.5889	3.0870	1.4894	0.6110	0.2622	0.2462
2	HSDT [23]	0.7572	3.6094	1.3954	0.5441	0.2763	0.2265
	Present	0.7573	3.6094	1.3954	0.5441	0.2763	0.2265
3	HSDT [23]	0.8372	3.8742	1.2748	0.5525	0.2715	0.2107
	Present	0.8377	3.8742	1.2748	0.5525	0.2715	0.2107
4	HSDT [23]	0.8810	4.0693	1.1783	0.5667	0.2580	0.2029
	Present	0.8819	4.0693	1.1783	0.5667	0.2580	0.2029
5	HSDT [23]	0.9108	4.2488	1.1029	0.5755	0.2429	0.2017
	Present	0.9118	4.2488	1.1029	0.5755	0.2429	0.2017
6	HSDT [23]	0.9345	4.4244	1.0417	0.5803	0.2296	0.2041
	Present	0.9356	4.4244	1.0417	0.5803	0.2296	0.2041
7	HSDT [23]	0.9552	4.5971	0.9903	0.5834	0.2194	0.2081
	Present	0.9562	4.5971	0.9903	0.5834	0.2194	0.2081
8	HSDT [23]	0.9741	4.7661	0.9466	0.5856	0.2121	0.2124
	Present	0.9750	4.7661	0.9466	0.5856	0.2121	0.2124
9	HSDT [23]	0.9917	4.9303	0.9092	0.5875	0.2072	0.2164
	Present	0.9925	4.9303	0.9092	0.5875	0.2072	0.2164
10	HSDT [23]	1.0083	5.0890	0.8775	0.5894	0.2041	0.2198
	Present	1.0089	5.0890	0.8775	0.5894	0.2041	0.2198
Metal	HSDT [23]	1.6071	1.9955	1.3121	0.7065	0.2132	0.2462
	Present	1.6070	1.9955	1.3121	0.7065	0.2132	0.2462

Table 4. Comparison of nondimensional critical buckling load $\hat{N}$ of isotropic plate under different loading types ($p = 0$)

a/b	h/b	Method	Loading type (x_1, x_2)		
			(-1,0)	(0,-1)	(-1,-1)
1	0.1	FSDT [38]	3.7865	3.7865	1.8932
		TSDT [38]	3.7866	3.7866	1.8933
		Present	3.7869	3.7869	1.8935
	0.2	FSDT [38]	3.2637	3.2637	1.6319
		TSDT [38]	3.2653	3.2653	1.6327
		Present	3.2666	3.2666	1.6333
	0.3	FSDT [38]	2.6533	2.6533	1.3266
		TSDT [38]	2.6586	2.6586	1.3293
		Present	2.6612	2.6612	1.3306
	0.4	FSDT [38]	1.9196	1.9196	1.0513
		TSDT [38]	1.9550	1.9550	1.0567
		Present	1.9651	1.9651	1.0586
1.5	0.1	FSDT [38]	4.0250	2.0048	1.3879
		TSDT [38]	4.0253	2.0048	1.3879
		Present	4.0258	2.0049	1.3880
	0.2	FSDT [38]	3.3048	1.7941	1.2421
		TSDT [38]	3.3077	1.7946	1.2424
		Present	3.3096	1.7951	1.2427
	0.3	FSDT [38]	2.5457	1.5267	1.0570
		TSDT [38]	2.5545	1.5285	1.0582
		Present	2.5580	1.5295	1.0589
	0.4	FSDT [38]	1.9196	1.2632	0.8745
		TSDT [38]	1.9421	1.2670	0.8772
		Present	1.9473	1.2686	0.8783
2	0.1	FSDT [38]	3.7865	1.5093	1.2074
		TSDT [38]	3.7866	1.5093	1.2075
		Present	3.7869	1.5094	1.2075
	0.2	FSDT [38]	3.2637	1.3694	1.0955
		TSDT [38]	3.2654	1.3697	1.0958
		Present	3.2666	1.3700	1.0960
	0.3	FSDT [38]	2.5726	1.1862	0.9490
		TSDT [38]	2.5839	1.1873	0.9498
		Present	2.5882	1.1879	0.9503
	0.4	FSDT [38]	1.9034	0.9991	0.7992
		TSDT [38]	1.9230	1.0015	0.8012
		Present	1.9292	1.0025	0.8020

Table 5. Comparison of nondimensional fundamental frequency $\check{S}$ of square plate

a/h	Method	Power law index (p)				
		0	0.5	1	4	10
5	FSDT [11]	0.2112	0.1805	0.1631	0.1397	0.1324
	HSDT [39]	0.2113	0.1807	0.1631	0.1378	0.1301
	Present	0.2113	0.1807	0.1631	0.1377	0.1300
10	FSDT [11]	0.0577	0.0490	0.0442	0.0382	0.0366
	HSDT [39]	0.0577	0.0490	0.0442	0.0381	0.0364
	Present	0.0577	0.0490	0.0442	0.0381	0.0364
20	FSDT [11]	0.0148	0.0125	0.0113	0.0098	0.0094
	HSDT [39]	0.0148	0.0125	0.0113	0.0098	0.0094
	Present	0.0148	0.0125	0.0113	0.0098	0.0094

Table 6. Comparison of the first four nondimensional frequencies $\check{S}$ of rectangular plate ($b = 2a$)

a/h	Mode (m,n)	Method	Power law index (p)						
			0	0.5	1	2	5	8	10
5	1 (1,1)	FSDT [11]	3.4409	2.9322	2.6473	2.4017	2.2528	2.1985	2.1677
		TSDT	3.4412	2.9347	2.6475	2.3949	2.2272	2.1697	2.1407
		Present	3.4416	2.9350	2.6478	2.3948	2.2260	2.1688	2.1403
	2 (1,2)	FSDT [11]	5.2802	4.5122	4.0773	3.6953	3.4492	3.3587	3.3094
		TSDT	5.2813	4.5180	4.0781	3.6805	3.3938	3.2964	3.2514
		Present	5.2822	4.5187	4.0787	3.6804	3.3914	3.2947	3.2506
	3 (1,3)	FSDT [11]	8.0710	6.9231	6.2636	5.6695	5.2579	5.1045	5.0253
		TSDT	8.0749	6.9366	6.2663	5.6390	5.1425	4.9758	4.9055
		Present	8.0772	6.9384	6.2678	5.6391	5.1378	4.9727	4.9044
	4 (2,1)	FSDT [11]	9.7416	8.6926	7.8711	7.1189	6.5749	5.9062	5.7518
		TSDT	10.1164	8.7138	7.8762	7.0751	6.4074	6.1846	6.0954
		Present	10.1201	8.7167	7.8787	7.0756	6.4010	6.1806	6.0942
10	1 (1,1)	FSDT [11]	3.6518	3.0983	2.7937	2.5386	2.3998	2.3504	2.3197
		TSDT	3.6518	3.0990	2.7937	2.5364	2.3916	2.3411	2.3110
		Present	3.6519	3.0991	2.7937	2.5364	2.3912	2.3408	2.3108
	2 (1,2)	FSDT [11]	5.7693	4.8997	4.4192	4.0142	3.7881	3.7072	3.6580
		TSDT	5.7694	4.9014	4.4192	4.0090	3.7682	3.6846	3.6368
		Present	5.7697	4.9016	4.4194	4.0089	3.7673	3.6839	3.6365
	3 (1,3)	FSDT [11]	9.1876	7.8145	7.0512	6.4015	6.0247	5.8887	5.8086
		TSDT	9.1880	7.8189	7.0515	6.3886	5.9765	5.8341	5.7575
		Present	9.1887	7.8194	7.0519	6.3885	5.9742	5.8324	5.7566
	4 (2,1)	FSDT [11]	11.8310	10.0740	9.0928	8.2515	7.7505	7.5688	7.4639
		TSDT	11.8315	10.0810	9.0933	8.2309	7.6731	7.4813	7.3821
		Present	11.8326	10.0818	9.0940	8.2306	7.6696	7.4787	7.3808
20	1 (1,1)	FSDT [11]	3.7123	3.1456	2.8352	2.5777	2.4425	2.3948	2.3642
		TSDT	3.7123	3.1458	2.8352	2.5771	2.4403	2.3923	2.3619
		Present	3.7123	3.1458	2.8353	2.5771	2.4401	2.3922	2.3618
	2 (1,2)	FSDT [11]	5.9198	5.0175	4.5228	4.1115	3.8939	3.8170	3.7681
		TSDT	5.9199	5.0180	4.5228	4.1100	3.8884	3.8107	3.7622
		Present	5.9199	5.0180	4.5228	4.1100	3.8881	3.8105	3.7621
	3 (1,3)	FSDT [11]	9.5668	8.1121	7.3132	6.6471	6.2903	6.1639	6.0843
		TSDT	9.5669	8.1133	7.3132	6.6433	6.2760	6.1476	6.0690
		Present	9.5671	8.1135	7.3133	6.6432	6.2753	6.1471	6.0688
	4 (2,1)	FSDT [11]	12.4560	10.5660	9.5261	8.6572	8.1875	8.0207	7.9166
		TSDT	12.4562	10.5677	9.5261	8.6509	8.1636	7.9934	7.8909
		Present	12.4565	10.5680	9.5263	8.6508	8.1624	7.9925	7.8905